DABCO cadmium(II) tetrakis(4-metoxyphenyl)porphyrin complex – Structure, photophysical properties, and adsorpion removal of methylene blue dye

Chadlia Mchiri, Abdelkader Ouakouak, Soumaya Nasri, Abdesslem Jedidi, Ilona Turowska-Tyrk, Samir Acherar, Céline Frochot, Thierry Roisnel, Habib Nasri

DABCO Cadmium(II) Tetrakis(4-metoxyphenyl)porphyrin Complex – Structure, Photophysical properties, and Adsorpion removal of methylene blue dye

Chadlia Mchiri[a,✉], Abdelkader Ouakouak[b], Soumaya Nasri[a,c], Abdesslem Jedidi[d], Ilona Turowska-Tyrk[e], Samir Acherar[f], Céline Frochot[g], Thierry Roisnel[h], Habib Nasri[a]

[a] Laboratoire de Physico-Chimie des Matériaux (LPCM), Faculty of Sciences of Monastir, Avenue de l'environnement,5019 Monastir, University of Monastir, Tunisia.
[b] Hydraulic and Civil Engineering Department, University of El Oued, PO Box 789, El Oued, 39000, Algeria.
[c] Department of Chemistry, College of Science Al-Zulfi, Majmaah University, Saudi Arabia.
[d] Department of Chemistry, Faculty of Science, King Abdulaziz University, Jeddah 21589, Saudi Arabia.
[e] Faculty of Chemistry, Wrocław University of Technology, Wybrze˙ze Wyspia´nskiego 27, 50-370 Wrocław, Poland
[f] Laboratoire de Chimie Physique Macromoléculaire (LCPM), Université de Lorraine, CNRS, 1 rue Grandville BP 20451, 54001Nancy Cedex, France.
[g] Laboratoire Réactions et Génie des Procédés (LRGP), Université de Lorraine, CNRS, 1 rue Grandville BP 20451, 54001 Nancy Cedex, France.
[h] Centre de Diffractométrie X, Institut des Sciences Chimiques de Rennes, UMR 6226, CNRS–Université de Rennes,1, Campus de Beaulieu, 35042 Rennes Cedex, France.

Abstract

In this work, a new cadmium(II) complex namely the (1,4-diazabicyclo[2.2.2]octane)(*meso*-tetrakis(4-tert-methoxyphenyl)porphyrinato)cadmium(II) with the formula [Cd(TMPP)(DABCO)] (**I**) (DABCO = 1,4-diazabicyclo[2.2.2]octane) was successfully synthetized. The structure of (**I**) have been characterized by FT-IR, ^{1}HNMR, UV-visible, fluorescence spectroscopies and single crystal X-ray diffraction technique. DFT calculations has been made for the structural, ^{1}H NMR spectroscopy and IR spectra analysis. The adsorption of methylene blue (MB) dye was studied to examine the efficiently of the [Cd(TMPP)(DABCO)] for removing the cationic dyes from aqueous solution. The Langmuir adsorption capacity (Q^{0}_{max}) at 290 K and pH 7.0 was found to be 69.24 mg.g^{-1}. The adsorption mechanism which involved π-π interaction between the MB dye molecule and the porphyrin ring of (**I**) is well described by the pseudo second-order and Elovich models.

Corresponding author. Fax: +216 73 500 278.
E-mail address: chadliamchiri@gmail.com(C. Mchiri).

Keywords: Cadmium porphyrin complex, DABCO ligand; Photophysical properties; Kinetic adsorption, Adsorption isotherms.

1. Introduction

For more than a half century, porphyrins and metalloporphyrins have attracted high interest from researchers due to their structural diversity and wide applications such as the organic catalysis [1], and the chemical sensing [2], in photodynamic therapy of cancers [3] and in solar photovoltaic cells [4]. Among the metalloporphyrins systems, the cadmium (II) porphyrins have been of general interest. Indeed, Cd (II) ion is too big to fit co-planarly into the cavity of porphyrin, it is located out of the ligand plane and distorts it. Therefore, the structure deformation of cadmium(II) metalloporphyrins results in kinetic lability making them good transmetalation precursors for metal-exchange reactions as well as peculiar photophysical and photochemical behavior [5-6]. Cd(II)-porphyrins are also of particular interest for some biological applications such as inhibition of DNA cleavage by HaeIII enzyme at high concentration (from 10^{-5} to 10^{-6} M), [7] induction of DNA conformational change [8] and anti-parasite activity on *Trypanosoma brucei brucei*. [9]. On the other hand, the environmental contamination caused by several organic dyes in many industries including textile, leather, paper, food, cosmetics, printing and plastics [10] has generate serious pollution with increasing industrialization and population. The remediation of dyeing industry wastewater can be accomplished by various physical and chemical methods such as photodegradation and adsorption processes. [11-14]. Among organic dyes, the methylene blue (MB) is one of the most used. This organic species is also named, methylthioninium chloride (Scheme 1), is a member of the thiazine class of dyes with many applications [15-16] which was first prepared by Heinrich Caro in 1876 [17]. Methylene blue is considered one of the most commonly used dyes that cause many health problems including vomiting, diarrhea, skin irritation, nausea and eye burns in human body, in addition to environmental pollution [18-19]. In recent years, the development of new materials has intensified in wastewater treatment due to their ability to remove various contaminants in water as well as efficient recovery of adsorbents after adsorption processes. Thus far, adsorption techniques have been widely used for the removal of dyes from aqueous solutions due to low-cost, regenerable, effective process and ease of operation [20]. Many types of adsorbent have been used of adsorption removal of dyes, such as hydrogels, clay minerals and carbon-based materials [21- 22].

It is worth noting that the use of porphyrins, metalloporpyrins and their derivatives in the removal of organic dyes by the absorption method has been the subject of a large number of publications in recent years [23-24]. During the last few years, our research group has published a number of works concerning the use of metalloporphyrins in adsorption removal of some organic dyes [25-27].

Continuing our work, in this paper, we synthesized a new cadmium(II) metalloporphyrine namely the (1,4-diazabicyclo[2.2.2]octane)[*meso*-tetrakis(4-tert-methoxyphenyl)porphyrinato]cadmium(II) with the formula [Cd(TMPP)(DABCO)] (**I**) (DABCO = 1,4-diazabicyclo[2.2.2]octane). The H_2TMPP free base porphyrin, the [Cd(TMPP)] and complex (**I**) were characterized by IR, ^{1}H NMR, UV-visible and

fluorescence spectroscopy. Theoretical study of the structure, ^{1}H NMR spectroscopy and IR spectra analysis of DABCO ligand, [Cd-TMPP] complex, and [Cd(TMPP)(DABCO)] complex (I) was investigated by DFT method at B3LYP/3-61G(d)/SDD level of theory.

Furthermore, our Cd-TMPP-DABCO species was studied by single crystal X-ray diffraction. An important part for the present work is dedicated to test the efficiency of complex (**I**) in the adsorption removal of the methylene blue dye in aqueous solutions. The efficiency of our adsorbent is also compared to other system used in the removal of the MB dye by adsorption procedures and the molecular modeling of the adsorption of MB dye on [Cd-TMPP-DABCO] (**I**) was described.

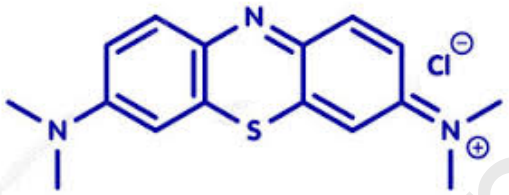

Scheme 1. Structure of the methylene blue dye (MB).

2. Materials and Methods

*2.1. Synthesis of [Cd(TMPP)(DABCO)]·1.5*$CHCl_3$·1.5$C_6H_{12}N_2$ (**I**)

In the present work, the *meso*-tetrakis(4-tert-methoxyphenyl)porphyrin (H_2TMPP) and the starting material complex [Cd(TMPP)] were synthesized, following literature methods [28-29]. The synthesis of [Cd(TMPP)(DABCO)] (**I**) was performed by dissolving [Cd(TMPP)] (25 mg, 0.03 mmol) in chloroform (2 mL). A saturated DABCO–chloroform solution (3 mL) was added. The mixture obtained was stirred for 12 hours then, 10 mL of n-hexane was added to the [Cd (TMPP)]-DABCO mixture. The resulting solution was left to infuse and crystallize for a minimum of 3 days, resulting in dark-purple crystals (yield 80%). The synthetic route to complex (**I**) is shown in Scheme 2.

Elemental analysis (%) calcd for $C_{57.5}H_{54.5}CdN_7O_4Cl_{1.5}$(1073.15 g/mol) C, 64.35; H, 5.11; N, 9.13%. Found: C, 64.68; H, 5.17; N, 9.19%. **UV-Vis** (CH_2Cl_2): [λ_{max} (nm) in CH_2Cl_2, (ε x 10^{-3}, mol^{-1} L cm^{-1})]: 440(307), 573(17),617(11). **IR** (cm^{-1}): 2987-2837ν $(CH)_{porph}$, 1511 ν$(C{=}C)_{porph}$, 1330 ν(C–N), 977 $(\delta CCH)_{porph}$, 1247ν$(O–CH_3)_{porph}$, **^{1}H NMR**(300 MHz, DMSO, 298 K): δ (ppm) 8.73 (s, 8H, H_{β}-pyrr.), 8.11 (s, 8H, H-o-Ph), 8.08 (s, 8H, H-m-Ph), 4.05 (s, 12H, O–CH_3).

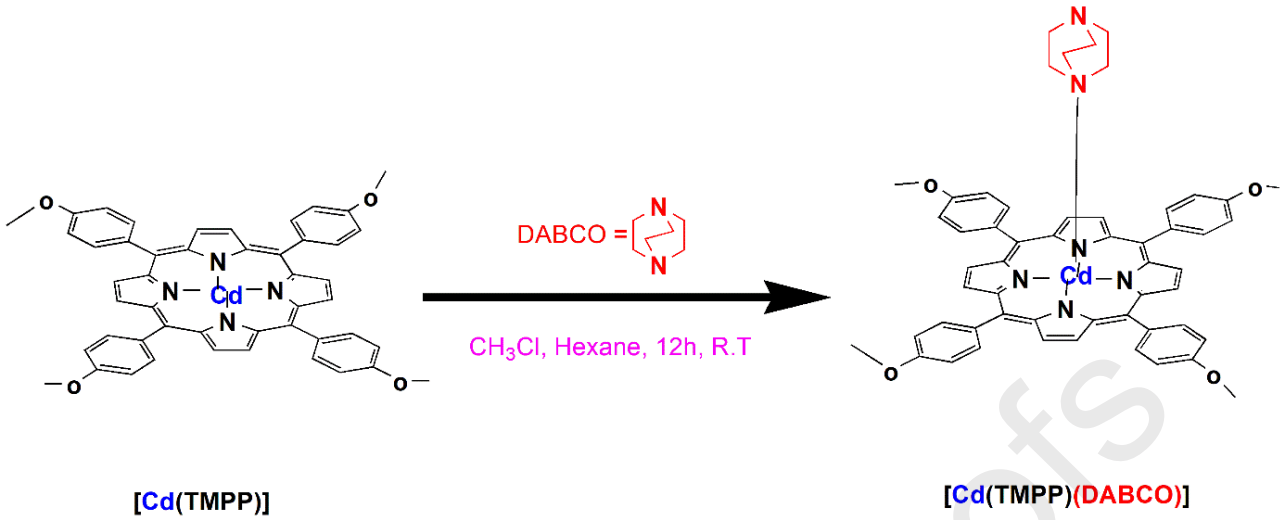

Scheme 2: Synthetic route to [Cd(TMPP)(DABCO)] complex (**I**).

2.2. Reagents

All reagents and solvents were commercially available, reagent grade, and used without further purification.

2.3. Spectroscopic and photophysical measurements

^{1}H NMR spectra were recorded on a Bruker AVANCE spectrometer (400 MHz). UV-Visible spectra were measured with a UV-3600 Shimadzu spectrophotometer. FT-IR spectra were recorded in the region of 400−4000 cm^{-1} on a Nicolet Impact 410 spectrophotometer. Fluorescence spectra were recorded on a Fluorolog-3 spectrofluorometer FL3-222 with a thermostated cell compartment (25 °C) using a 450 W Xenon lamp. Fluorescence quantum yield (φ_f) were determined using tetraphenyl porphyrin (H_2TPP) solution in toluene as fluorescence standard ($\varphi_f = 0.11$) [30].

2.4 Crystal structure determination

A suitable crystal of [Cd(TMPP)(DABCO)] complex (**I**) were chosen and their X-ray analysis were done using the unit-cell parameters were calculated and refined from the full data and the data collection was performed with a Bruker D8 VENTURE diffractometer at 150 K. Data were corrected for absorption effects by the Multi-Scan method [31]. The structure was solved by direct method by using SIR-2004 program [32] and refined by full-matrix least-squares techniques on F^2 by using the SHELXL-97 program [33]. The structure was refined as an inversion twin with a final BASF parameter of 0.430 (2). One chloroform and one n-hexane solvent molecules located in a very close positions were refined with a 50%/50% occupation ratio. The anisotropic displacement ellipsoids (ADPs) of the chloroform solvent molecule and the free DABCO molecules are very elongated; therefore, there is static disorder in the molecular structure of (**I**). For fragments involving these

atoms, the DFIX, DANG, and SIMU constraint commands in the SHELXL-97 software were used [34]. The ADPs of the atoms of the DABCO axial ligand (C59-C62- C64) exhibits also high ADPs values for which the ISOR and SIMU constraint commands were applied. The drawings were made with Mercury [35]. Crystal data and details of the structure determination are summarized in Table S1 (Supplementary Materials). Selected bond lengths and angles of complexes are listed in Table 1. Crystallographic data have been deposited as supplementary publication number CCDC No 2012300.

2.3. Adsorption experiments and data analysis

Tests of methylene blue dye adsorption onto [Cd(TMPP)(DABCO)] were carried out in a batch manner. Briefly, 6 mg of adsorbent was dispersed in Erlenmeyer flasks containing 20 mL of MB dye solution at known concentration. Then, the mixture was stirred (at 200 rpm) during the desired time. After filtering the solution through a 0.45 µm membrane filter, the residual MB content was determined by UV-visible spectrophotometer. The characteristic peak for methylene blue was (~ 664 nm) has been employed to monitor the adsorption. All tests of MB dye adsorption were performed at pH = 7.0 ± 0.1. The removed quantity of MB dye from solution at any time t (q_t, mg/g) and at equilibrium (q_e, mg/g) were calculated by the following equations **(1-2)**:

$$q_t = (C_0 - C_t) * V / m \qquad \textbf{(1)}$$

$$q_e = (C_0 - C_e) * V / m \qquad \textbf{(2)}$$

where C_0, C_t and C_e (mg/L) are the MB dye concentration at beginning, at time t, and at equilibrium, respectively. V (L) is the volume of MB dye solution whereas m (g) represents the mass of adsorbent used.

In order to investigate the MB dye adsorption mechanisms onto [Cd(TMPP)(DABCO)], three common models of kinetics and isotherms were selected for modelling the experimental data. The non-linear forms of the pseudo-first-order (PFO) [36], the pseudo-second-order (PSO) [37] and the Elovich [38] kinetic models are given by equations **(3-5)**, respectively.

$$q_t = q_e\left(1 - e^{-k_1 t}\right) \qquad \textbf{(3)}$$

$$q_t = \frac{q_e^2 k_2 t}{1 + q_e k_2 t} \qquad \textbf{(4)}$$

$$q_t = \frac{1}{\beta}\ln(1 + \alpha\beta t) \qquad \textbf{(5)}$$

where q_t, q_e, and C_e are defined above in Equations **(1)-(2)**, k_1 (L/min) is the rate constant of PFO equation; k_2 (g/mg × min) is the PSO rate constant; α (mg/g × min) is the initial adsorption rate of Elovich model; and β (mg/g) is the desorption constant during any one experiment.

To describe the adsorption isotherm, the non-linear forms of Langmuir [39], Freundlich [40] and Redlich-Peterson [41] models are given by Equations **(6-8)**, respectively:

$$q_e = \frac{Q^o_{\max} K_L C_e}{1 + K_L C_e} \quad \textbf{(6)}$$

$$q_e = K_F C_e^n \ \textbf{(7)}$$

$$q_e = \frac{K_{RP} C_e}{1 + a C_e^g} \quad \textbf{(8)}$$

where Q^o_{max} (mg/g) is the maximum monolayer capacity of Langmuir; K_L (L/mg) is the Langmuir affinity constant; K_F (mg/g)(L/mg)^n represents the Freundlich constant; n (dimensionless; $0< n <1$) is the intensity parameter of Freundlich; K_{RP} (L/g) and a_{RP} (mg/L)$^{-g}$ refer to the Redlich–Peterson constants and g (dimensionless) is an exponent which must be between 0 and 1.

In this study, the Origin software was used to calculate the relevant parameters of all models by applying the non-linear technique.

The difference between the experimental and calculated values of the adsorbed quantity (q_e and q_t in mg/g) was evaluated using the coefficient of determination (R^2) and the chi-square test (χ^2) [42].

$$R^2 = 1 - \frac{\sum (q_{e,\exp} - q_{e,cal})^2}{\sum (q_{e,\exp} - q_{e,mean})^2} \quad \textbf{(9)} \quad \chi^2 = \sum \frac{(q_{e,\exp} - q_{e,cal})^2}{q_{e,cal}} \ \textbf{(10)}$$

where $q_{e,mean}$ (mg/g) is the mean of q_e experimental $(q_{e,exp})$ values and $q_{e,cal}$ (mg/g) is the adsorbed quantity determined from the selective model.

2.4. Computational details

All the calculations were performed using the Gaussian09 suites [43] and monitored by Gaussview Software [44]. The density functional theory (DFT) method has been applied with the B3LYP functional [45] in connection with a valence double-zeta (6-31G) basis set, adds to the **6-31G basis set** five d-type Cartesian-Gaussian polarization functions on each of the atoms C, N, O, S, Cl and H [46], and the SDD basis set for Cd metal [47]. No symmetry constraints were used in the geometry optimizations, and the final geometries were confirmed to be minimum potential energy structures through frequency calculations. Weak interactions have been included in the energy evaluation using 'Empirical Dispersion' option with Grimme D3 corrections. The effect of solvent (water) on the relative stabilities was calculated using the Tomasi's polarized continuum (PCM) model [48]. The calculation of NMR spectrum of the different structures was performed using the GIAO (Gauge-Including Atomic Orbitals) method [49].

3. Results and discussion

3.1. Crystal Structures of [*Cd(TMPP)(DABCO)]·1.*5$CHCl_3$·1.5$C_6H_{12}N_2$ (**I**)

Single crystal X-ray diffraction analysis reveals that complex (**I**) crystallizes in the triclinic *P-1* space group with Z=2. Crystallographic data and structure refinement are reported in Table S1. The asymmetric unit contains one molecule of [Cd(TMPP)(DABCO)], one half chloroform and one half DABCO molecules. The ORTEP drawings of the molecular structure of complex [Cd(TMPP)(DABCO)] is shown in Figure 1 and the main geometrical parameters are listed in Table 1.

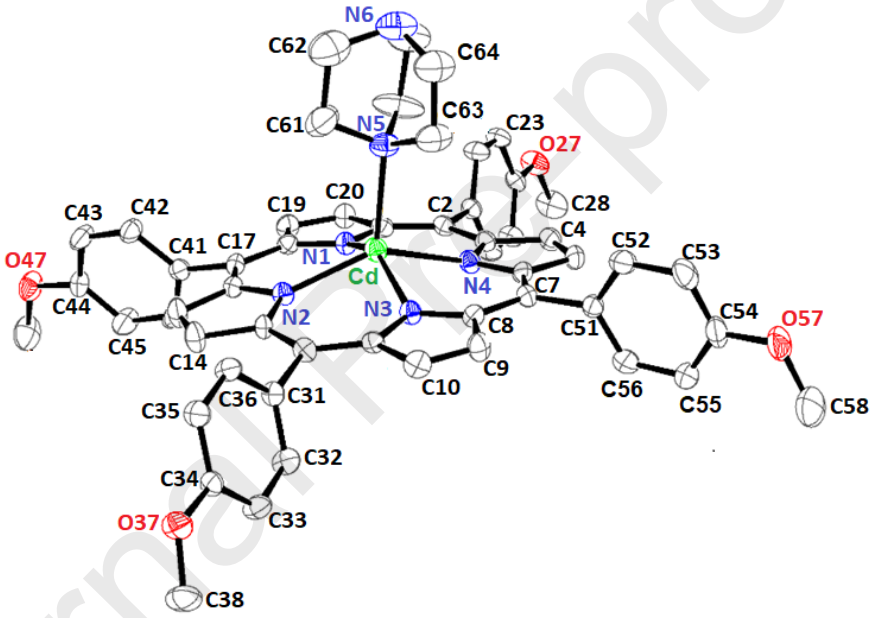

Figure 1. ORTEP diagram and numbering scheme of [Cd(TMPP)(DABCO)]. The hydrogen atoms are not represented for clarity. 30% probability surfaces.

The central cadmium is linked by four N-donor nitrogen atoms of the tetradentate deprotonated porphyrin ligand ($TMPP^{2-}$), and axially by the nitrogen atom of the DABCO axial ligand leading to a pentacoordinate Cd(II) porphyrin complex. Table 1 lists the selected bond lengths and angles.

Table 1. Selected bond lengths (Å) and angles (deg) of [Cd(TMPP)(DABCO)]·1.5$CHCL_3$·1.5$C_6H_{12}N_2$ (**I**)

Cadmium(II)coordination polyhedron			
Cd–N1	2.188(6)	N1–Cd–N2	85.6(2)
Cd–N2	2.204(4)	N1–Cd–N3	146.41(16)
Cd–N3	2.177(6)	N1–Cd–N4	85.4(2)
Cd–N4	2.194(4)	N1–Cd–N5	105.5(2)
Cd–N5	2.319(5)	N2–Cd–N5	99.18(18)
		N3–Cd–N5	107.8(2)
DABCO Ligand			
N5–C60	1.441(1)	N3– Cd1–N5	107.8(2)
N5–C63	1.463(11)	N1– Cd1–N5	105.5(2)
N5–C61	1.492(10))	N4– Cd1– N5	114.79(17
N6–C59	1.389(14)	N2– Cd1– N5	99.18(18)
N6–C63	1.392(15)		
N6–C62	1.473(13)		

The average equatorial distance between the Cd^{2+} central ion and the four nitrogen atoms of the pyrrole rings (Cd—N_p) is in the normal range of pentacoordinate Cd(II) metalloporphyrins with a value of 2.192(5) Å (Table 2). The Cd—$N_{(DABCO)}$ bond length [2.320(5) Å] is considerably close to those of the reported related five-coordinate Cd(II) porphyrin complexes (Table 2).

The geometry of any penta-coordinated metal center may conveniently be measured by the Addison parameter (τ) [50]. The value of τ is defined as the difference between the two largest Ligand–Metal–Ligand angles divided by 60, [τ = (Θ−Φ)/60, where Θ and Φ are the two largest of the coordination sphere], τ is 0 for the ideal square pyramid and 1 for the trigonal bipyramid. In the present complex, the τ values of Cd center was calculated to be 0.52 indicating a distorted square-pyramidal geometry. The Addison parameter τ of (**I**) is close to those of reported Cd(II)-porphyrin complexes with N-donor of axial ligands (such as pyridine and 2-NH_2-pyridine).

Table 2. Experimental and theoretical study of the structural parameters: bond lengths (Å)[a] and angles (°) of [Cd(TMPP)(DABCO)]·1/2$CHCl_3$·1/2$C_6H_{12}N_2$(**I**) and several related five-coordinate cadmium porphyrin complexes

Complex		**Cd-N_p** [b]	**Cd•••P_{Ct}** [c]	**Cd-N_{ax}** [d]	**τ= (Θ−Φ)/60**	**Ref.**
[Cd(TMPP)(DABCO)]	Exp.	2.192(5)	0.746	2.320(5)	0.52	this work
	Theor.	2.255	0.770	2.360		
[Cd(TBPP)(2-MeHIm)][e]		2.215(7)	0.860	2.31(4)/2.278(6)	0.38	[51]
[Cd(TClPP)(py)][f]		2.203(4)	0.729	2.316(4)	0.51	[52]
[Cd(TClPP)(DMF)][g]		2.197(8)	0.824	2.280(2)	0.67	[52]
[Cd(TPP)(pip)][h]		2.203(3)	0.751	2.323 (2)	0.53	[53]

[Cd(TPP)(4-picoline)]	2.195	0.744	2.298	0.66	[54]
[Cd(TPP)(2-NH_2-py)][i]	2.204(3)	0.739	2.316(3)	0.53	[55]
[Cd(TPP)(N_3)][j]	2.215(1)	0.796	2.238(2)	0.40	[56]

[a]**:** Estimated standard deviations are given in parentheses, [b]**:** Cd-N_p is the average equatorial Cd-pyrrole nitrogen bond length,[c]: Cd•••P_{Ct} is the displacement of the Cd metal atom out of the porphyrinato mean plane, [d]**:** Cd-N_{ax} is the Cd-axial ligand bond length.[e]: 2-MeHIm: 2-methylimidazole, [f]**:** py: pyridine, [g]: DMF: N,N-diméthylformamide, [h]: pip: piperidine, [i]: 2-NH_2-py: 2-aminopyridine.

Furthermore, the planarity of porphyrin core has been analyzed and as shown in Figure 2. The Cd(II) cation of (**I**) has a large atomic radius which implies that central ion is too large to fit into the central hole of the porphyrin with a distance between the cadmium atom and the mean plane made by the 24-atom core of the porphyrin (Cd–P_C) of 0.746 Å, in agreement with DFT calculations showing a distance of 0.770 Å. This high value induces a significant porphyrinato core *doming* which is similar to those of the related five-coordinated cadmium metalloporphyrin with *N*-donor axial ligand (Table 2).

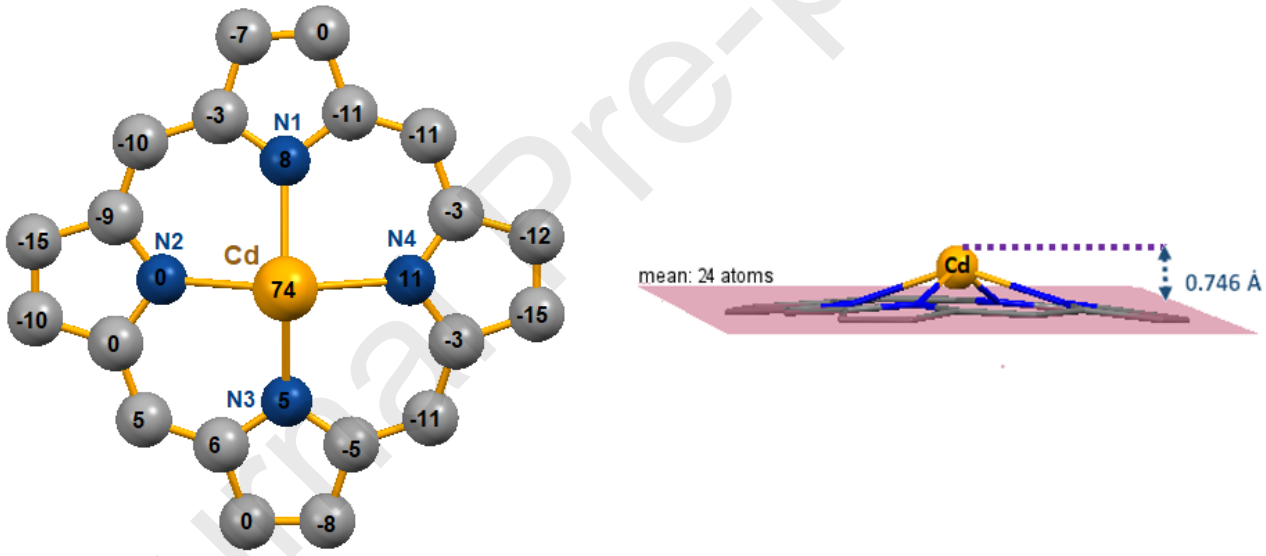

Figure 2. Formal diagrams of the porphyrinato core showing the *Doming* distortion in [Cd(TMPP)DABCO] complex (**I**)

The crystal lattice of complex (**I**) shows hydrogen intermolecular interactions between C-H···N and C-H···O." Indeed, the hydrogen atom, H(55) attached to the phenyl carbon atom, C55, is involved in a intermolecular C–H···N interaction with the nitrogen atom N6 of the coordinated DABCO axial ligand with a C55–H55···N6 distance of 2.35(14) Å. Two other hydrogen atoms, H(H69A) and H(H69B), attached to the carbon atom C(69) of the non-coordinated DABCO molecule, are also

involved in other intermolecular C−H···O interactions with the oxygen of the methoxy group of TMPP. These three different types of interactions lead to a pseudo-2D superstructure (Figure 3). Details of the geometric features of C−H···X (X = N, O) interactions in crystal lattice of (**I**) are given in Table 3.

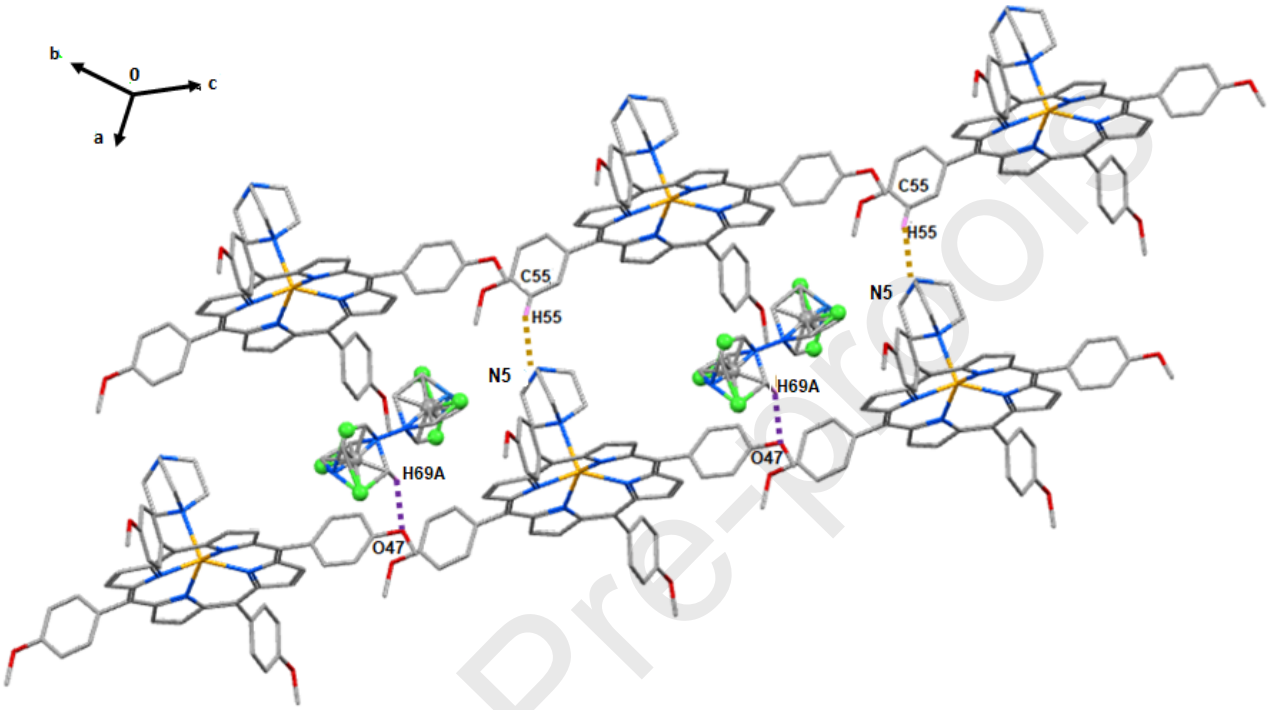

Figure 3. Schematic representation of the pseudo-2D supramolecular architecture of complex (**I**) via C–H···N and C–H···O interactions. Only relevant atoms have been shown.

Table 3. Geometric features (distances in Å and angles in °) of the intramolecular interactions for (**I**).

D[a]–H …A[b]	Symmetry of A	D-H…A [Å]	D…A [°]
C69 –H69A…O47	-x,-y,1-z	147	2.48(3)
C69 –H69B…O37	1-x,1-y,2-z	161	2.46(3)
C55-H55…N6	1+x,y,z	152	2.35(13)

[a]: D is the donor atom, [b]: A is the acceptor atom.

3.2. Molecular modeling of the complexes

The Cd-TMPP complex has been modeled in order to study the formation of [Cd-TMPP-DABCO] complex (I). Geometry optimization and vibrational frequencies have been performed at B3LYP/6-31G(d)/SDD level of theory. The structural analysis (bond lengths and angles) is shown in Table S2 and the IR spectra is presented in Figure 4.

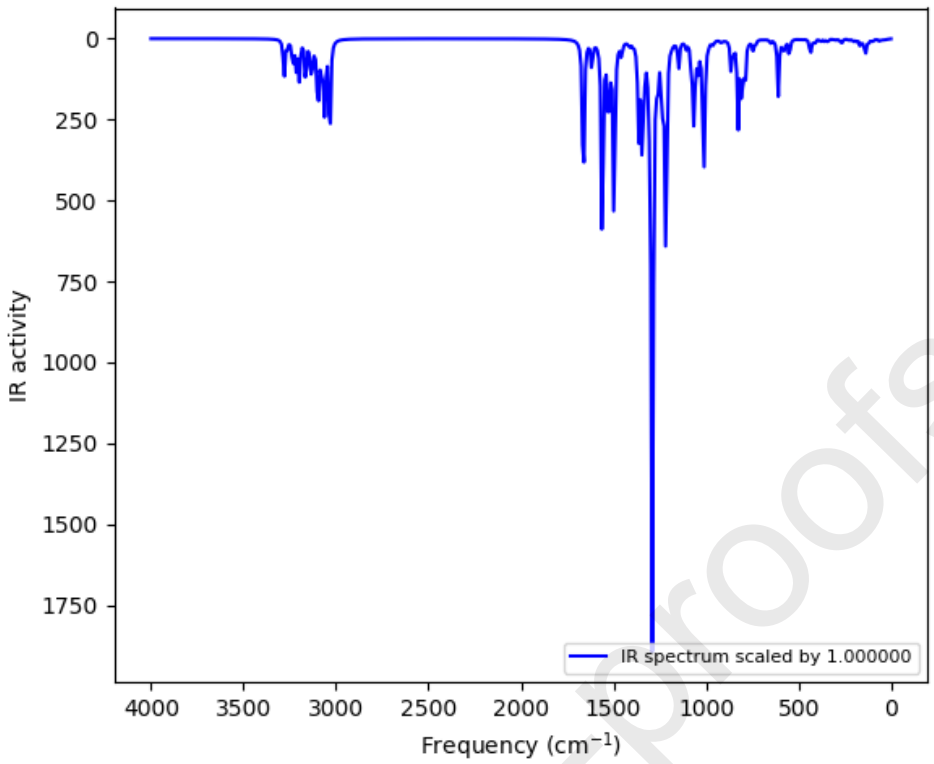

Figure 4. Theoretical IR spectra of the complex (I).

The IR spectra display mainly similar peaks associated with the two complexes [Cd-TMPP] and [Cd-TMPP-DABCO]. They experience shifts of 1-2 cm-1 for C–C and C=C bonds and around 34 cm-1 for C-H bond. Calculated IR spectra is in agreement with the experimental values (see Table 4).

Table 4. IR assignments of the [Cd-TMPP] and [Cd-TMPP-DABCO] complexes

Measured (theoretical)*			Assignment
[Cd-TMPP]	**[Cd-TMPP-DABCO]**	**[Cd-TMPP-DABCO-MB]**	
1247 (1289)	1247 (1289)	1247 (1290)	(O–CH_3)
- (1262)	- (1261)	- (1263)	(C–C)
1511 (1532)	1511 (1534)	1511 (1530)	(C=C)
- (3033)	- (3033)	- (3033)	$(C\text{-}H)_{methyl}$
	- (3062)	- (3066)	$(C\text{-}H)_{DABCO}$
		- (3270)	$(C\text{-}H)_{MB}$
- (3196-3200)	2837-2987 (3196-3234)	2837-2987 (3198-3236)	$(C\text{-}H)_{proph}$
- (3283)	- (3279)	- (3282)	$(C\text{-}H)_{pyrrol}$
- (1284)	- (1285)	- (1285)	$(C{=}N)_{asym}$
- (1305)	- (1307)	- (1305)	$(C{=}N)_{sym}$
- (1014)	- (1008)	- (1009)	$(Cd\text{–}N_p)$**

(*) From the DFT vibrational frequency calculations
**Cd-Np is the average equatorial Cd-pyrrole nitrogen bond length

3.3. Electronic and emission spectra of complex (I)

The porphyrins and metalloporphyrins have a π strongly conjugated electron system. These molecules absorb in the visible range and have characteristic absorption spectra induced by π → π* transitions. The first one involves the transition from the ground state (S_0) to the second excited state (S_2). corresponding to the B band (known as the Soret band). The range of the $S_0 \rightarrow S_2$ absorption band s between 380-500 nm depending on whether the porphyrin is β- or *meso*-substituted. The second region consists of a weak π → π* transition corresponding to the $S_0 \rightarrow S_1$ transition from the ground state to the first excited state in the range between 500-750 nm (the Q bands).

The electronic spectra, recorded in dichloromethane of the free base porphyrin H_2TMPP, the [Cd(TMPP)] starting material and complex (**I**) are depicted by Figure 5. The absorption data of these species and several other related Cd(II) *meso*-arylporphyrins are summarized in Table S3. The λ_{max} values of the Soret and Q bands of the free base H_2TMPP are 422nm and 518, 555, 594, 650, respectively. After metallation of the porphyrin by the cadmium ion, the color changes from purple to green and the number of the Q bands decreases from four to two due to the symmetry change from D_{2h} to D_{4h}. The color change is due to the important redshift of the Soret band from 422 nm for the H_2TMPP to 437 nm for the [Cd(TMPP)] starting material. The Q bands of this complex are also redshifted (573, 617 nm) compared to those of the free base porphyrin (518, 555, 594 and 650 nm) (Figure 5). The coordination of the DABCO to the Cd(II) ion of the tetracoordinated starting material leads a slightly redshift of both the Soret and the Q bands (Figure 4, Table S3). Notably, the important bathochromic shift of the absorption bands is related to the deformation of the porphyrin core [57].

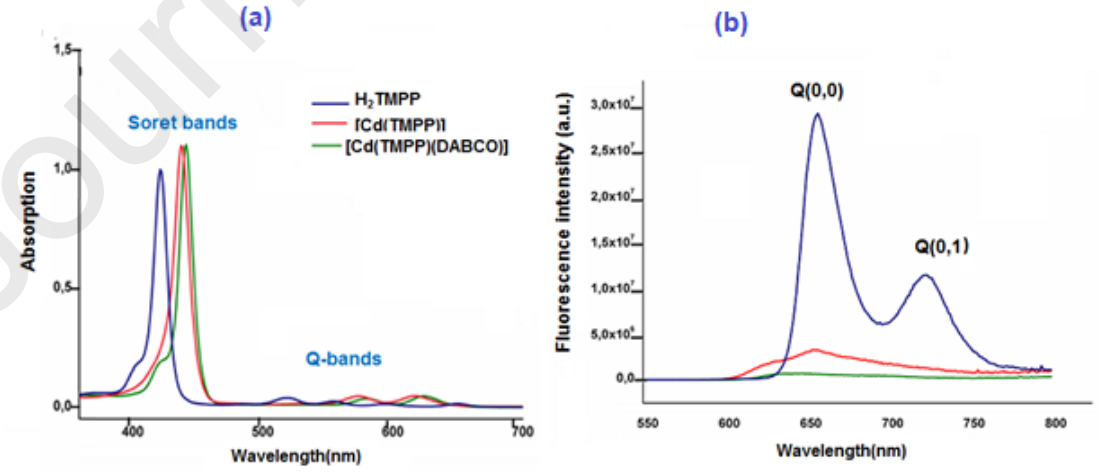

Figure 5. **(a)** UV-Visible spectra of H_2TMPP, [Cd(TMPP)] and complex (**I**) in CH_2Cl_2 (c~ 10^{-5} M), **(b)** fluorescence emission spectra of the same three porphyrinic species in CH_2Cl_2 (c~ 10^{-6} M), excitation λ_{exc}=437 nm.

The fluorescence emission spectra of the free base porphyrin H_2TMPP, and its cadmium complexes at room temperature were recorded in dichloromethane ($c\sim 10^{-6}$ M) upon photoexcitation at the wavelength 437 nm leads to forming two emission bands $S_1 \rightarrow S_o$ allocated as the Q(0,0) and Q(0,1) transitions. The fluorescence parameters, i.e. the λ_{max} fluorescence wavelength values of the Q (0,0) and Q (0,1) bands, and the fluorescence quantum yields (Φ_f), as well as the fluorescence lifetimes ($\boldsymbol{\tau}_f$) of H_2TMPP, [Cd(TMPP)] and complex (**I**) are listed in Table S4.

As shown by Figure 5b the heavy diamagnetic ion Cd(II) leads to weak fluorescence, the cadmium insertion resides in a very important hypsochromic shifts of ~ 50 nm for the strongest emission band Q(0,0), and ~ 60 nm for the second band Q(0,1 accompanied by a highly important reduction in the fluorescence intensity. This quenching of the fluorescence is explained by the "heavy-atom effect" of the cadmium heavy metal and the distortion of the porphyrin core, which promotes the loss of the "motion energy" by other non-radiative energy dissipation processes than light emission [58-59].

3.4. Adsorption removal of methylene blue (MB) dye

3.4.1. Adsorption

The adsorption of the MB dye on our synthetic cadmium(II)-DABO derivative was carried out at room temperature in aqueous solutions and the adsorption spectra of MB dye as a function of time in presence of (**I**) are shown in Figure S1 (supplementary information). As shown in this figure, the main absorption band (λ_{max} = 664 nm) of the BM dye decreases after adding complex (**I**) as function of time and almost disappears after 120 min of stirring time.

It has been reported that in the case of the porphyrin-based porous organic polymer (PPOPs-OH) [60], the π-π interactions (of the porphyrin macrocycle) is one of the driving force of the adsorption phenomenon. In our case, the adsorption phenomenon is most probably due to the fact that complex (**I**) is coordinated to a very aromatic ligand which is the meso-tetrakis(4-tert-methoxyphenyl)porphyrin and to the cyclic N-donor ligand DABCO. Therefore, the adsorption of the dye on (I) involves π-π interactions and probably weak H bonds and van der Waals interactions involving the MB due molecule and our cadmium-DABCO-TMPP porphyrin coordination compound.

3.4.2. Kinetic Adsorption

As mentioned in the experimental section, three kinetic models have been used study the MB dye adsorption on complex (**I**) which are the non-linear forms of the pseudo-first-order (PFO) [36], the pseudo-second-order (PSO) [37] and the Elovich [38]. The adsorption capacity curves as function of time for our Cd(II)-DABCO derivative (**I**) are given in Figure 6 which shows that the adsorption rate

of MB dye increases with increasing stirring time and the equilibrium (or saturation) is reaches after about 60 min of the contact of MB dye with (**I**). It can be seen from the curves given in Figure 6 that the adsorption mechanism is speedy, with around 80.7% of total MB dye in the solution being adsorbed within 15 min of stirring time.

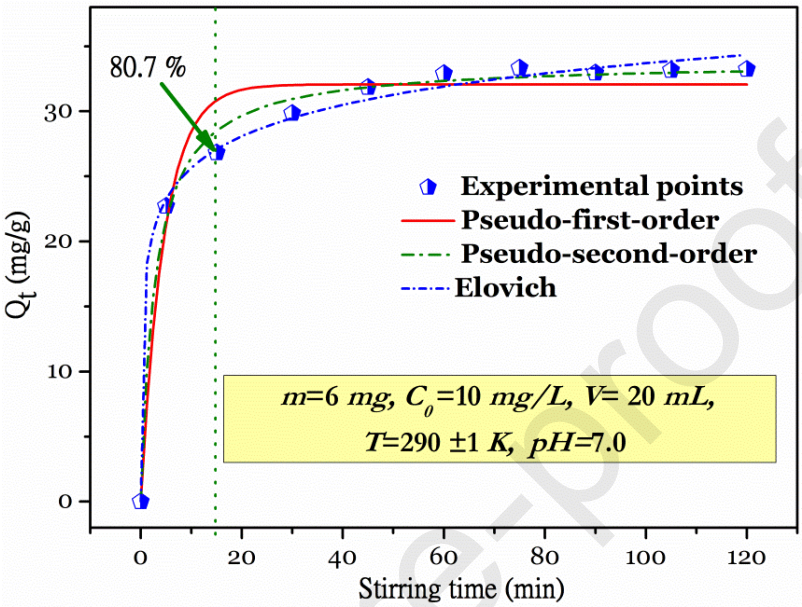

Figure 6. MB dye (C_o =10 mg.L^{-1}) as a function of time for complex (**I**) (m = 6 mg, pH = 7.0). Dots represents the experimental data and the curves where plotted using the pseudo-first-order, the pseudo-second-order and the Elovich models.

The results obtained using the three models which were evaluated based on the regression coefficient R^2 and chi-square (χ^2) values, given in Table 5, indicate that the experimental results are better fitted using the Elovich and the PSO models with R^2/ χ^2values of 0.994/0.577 and 0.993/0.766 respectively. This finding is also well confirmed by the fitting lines presented in Figure 6.

Table 5. Kinetic data for the adsorption of MB dye using complex (**I**) (Co = 10 mg L^{-1}, pH = 7.0, m = 6 mg)

Model	Parameter	Unit	Value	Standard Error
PFO	k_1	L/min	0.218	0.035
	q_e	mg/g	32.06	0.696
	R^2	—	0.966	—
	χ^2	—	3.605	—
PSO	k_2	g/mg×min	0.010	0.001
	q_e	mg/g	33.85	0.428
	R^2	—	0.993	—

	χ^2	—	0.766	—
Elovich	α	mg/g × min	542.84	317.75
	β	mg/g	0.286	0.021
	R^2	—	0.994	—
	χ^2	—	0.577	—

3.4.3. Adsorption isotherm

In this study, Langmuir, Freundlich and Redlich-Peterson models are used to analyze the equilibrium data of MB adsorption. The fitting curves of the studied models are displayed in Figure 7. In addition, Table 6 summarizes the relevant parameters for the previously mentioned models.

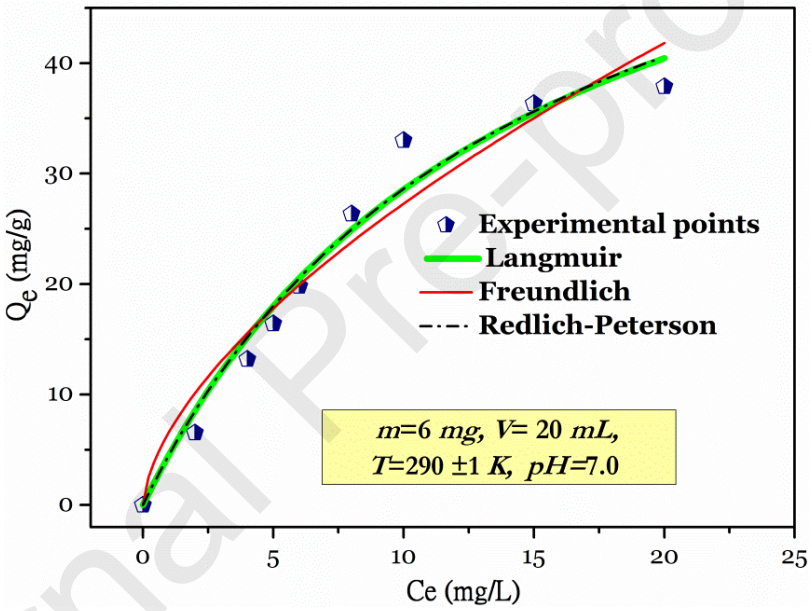

Figure 7. Adsorption isotherms of MB dye onto [Cd(TMPP)(DABCO)] (**I**) and fitting curves of the selective models.

In the light of R^2 and χ^2 values, Langmuir gives the best fit of the experimental data of adsorption isotherm at 298 K because it exhibits the highest R^2 and the lowest χ^2 values, in comparison with Freundlich and Redlich-Peterson models (Table 6).This finding suggests a monolayer adsorption of MB molecules onto homogeneous surface of [Cd(TMPP)(DABCO)] adsorbent. Furthermore, the maximum adsorption capacity was found to be 69.24 $mg.g^{-1}$ according to the Langmuir equation.

Table 6. Parameters of adsorption isotherms of MB dye on [Cd (TMPP) (DABCO)] (**I**) adsorbent.

Model	Unit	Value	Standard Error
Langmuir			
Q^{o}_{max}	mg/g	69.24	10.23
K_L	L/mg	0.070	0.018
R^2	—	0.968	—
χ^2	—	5.71	—
Freundlich			
K_F	$(mg/g)/(mg/L)^n$	6.60	1.34
n	—	0.616	0.080
R^2	—	0.938	—
χ^2	—	10.97	—
Redlich–Peterson			
K_{RP}	L/g	4.86	2.284
a_{RP}	$(mg/L)^{-g}$	0.070	0.194
g	—	0.988	0.683
R^2	—	0.963	—
χ^2	—	6.27	—

3.4.3. Comparison of our adsorption results with other reported investigations

Many investigations concerning the MB dye adsorption have previously been reported in the literature (Table 7). As depicted in this table, the removal yield and the capacity of adsorption (Q_{max}) using our Cd(II) porphyrin derivative [Cd(TMPP)(DABCO)] (**I**) with values: Q_{max} = 69.24 mg.g-1 and 80.7% yield, are slightly better than those of the two first examples reported in Table 7 of non-porphyrinic systems used to remove the MB dye. By the other hand, the adsorption removal systems, reported in the same Table 7, using a poloxometallate and porphyrin base compounds exhibits higher adsorption capacities and yields that our synthetic complex (**I**). Nevertheless, in our case we used a low concentration of the MB dye ringing from 2 to 10 $mg.L^{-1}$ which is not the case of the other adsorbents reported in Table 7. Indeed, in the case of the related porphyrinic absorbents such as the "Porphyrin-calcium $\{[Ca(HDCPP)_2(DMF)_2]_n$ polymer" [61] and the "Porphyrin-based porous organic polymer (PPOPs-OH) " [60] , the dye concentrations are 15 and 50 $mg.L^{-1}$, respectively. Therefore, the results obtained by using complex (**I**) indicate the prominent potential of our Cd(II) porphyrinic system for dye treatments.

Table 7. Comparison of the adsorption removal of MB dye

Absorption system	Experiment conditions	Yield, Q_{max}, reaction time	Ref.
Corncobs from Pakistan particle sizes (105–400 µm)	$[MB]_0$ = 30–300 mg L−1. 303 K, m = 0.05 g, pH = 6.8	Q_{max} = 45.86 mg.g^{-1} 91.7%, 200 min	[62]
Raw bentonite (Algeria)	$[MB]_0$ = 10 mg L^{-1}. 293 K, m = 0.015 g, pH > 7	Q_{max} = 65.36 mg.g^{-1} 60 min	[63]
Keggin-type Polyoxometalate, $[Cu\{(HOCH_2CH_2)_2(NCS)_2\}_2]_3[PW_{12}O_{40}]$	$[MB]_0$ = 25 mg L^{-1}. 298 K, m = 45 mg	95% yield, 50 min	[64]
Porphyrin–calcium, Polymer $\{[Ca(HDCPP)_2(DMF)_2]_n$[a]	$[MB]_0$ = 15 mg L^{-1}. 298 K, m =5 mg	Q_{max} = 952 mg.g^{-1} 180 min	[61]
Porphyrin-based porous organic polymer (PPOPs-OH)	$[MB]_0$ = 50 mg L^{-1}. 298 K, m =5 mg	Q_{max} = 980.4 mg.g-1 100 min.	[60]
[Cd(TMPP)(DABCO)] ·1.5$CHCL_3$·1.5$C_6H_{12}N_2$	$[MB]_0$ = 10 mg.L^{-1}. 298 K, m = 6 mg, pH = 7	Q_{max} = 69.24 mg.g^{-1} Yield = 80.7%, 20 min	this work

[a]: H_2DCPP = 5,15-di(4-carboxyphenyl) porphyrin.

*3.4.3. Molecular modeling of the adsorption of MB dye on (Cd-TMPP-DABCO] complex (**I**)*

The interaction of MB dye with both [Cd-TMPP] and [Cd-TMPP-DABCO] complexes has been performed in order to calculate the adsorption energy for each case (Table 8). We calculated first the interaction between the DABCO ligand and the [Cd-TMPP] complex (Figure x). Then, we performed the adsorption of MB dye on an isolated [Cd-TMPP] complex and also in presence of DABCO (complex I). The former adsorption was made for the sake of comparison of the interaction strength. The adsorption energy of DABCO on the [Cd-TMPP] (complex I) is found -18.3 kcal/mol, that is lower than the adsorption of MB dye on the same complex (complex II) by 5.6 kcal/mol (E_{ads}= -12.3 kcal/mol). The adsorption energy of the MB dye in presence of DABCO is higher than the sum of the interactions between MB and DABCO with [Cd-TMPP] complex, respectively. The difference may be due to the repulsion generated between te MB dye and DABCO ligand.

Table 8. Adsorption energy (kcal/mol) of the three considered complexes (I-III)

System	Total Energy+D3 (H)	E_{ads} (kcal/mol)
Cd-TMPP	-2538.570	
DABCO	-345.351	
MB	-1643.244	
Complex (I)	-2883.950	-18.3
Complex (II)	-4181.835	-12.7
Complex (III)	-4527.203	-23.6

(I) Cd-TMPP-DABCO, **(II)** Cd-TMPP-MB, and **(III)** Cd-TMPP-DABCO-MB complex.

3.4.4. FT-IR Characterization

The FT-IR spectra of [Cd(TMPP)(DABCO)], MB, and MB-[Cd(TMPP)(DABCO)] species are depicted in Figures 8 and S3 and the characteristic absorption bands are listed in Table 9. Inspection of Figures 9 and S3 shows that the characteristic absorption bands of the "MB [Cd(TMPP)(DABCO)] " species are shifted compared to those of [Cd(TMPP)(DABCO)] and the MB dye before adsorption (Table 9). These finding confirm the adsorption of the dye by our Cd(II) adsorbent (**I**).

The Theoretical data of the absorption bands are in in agreement with the experimental data.

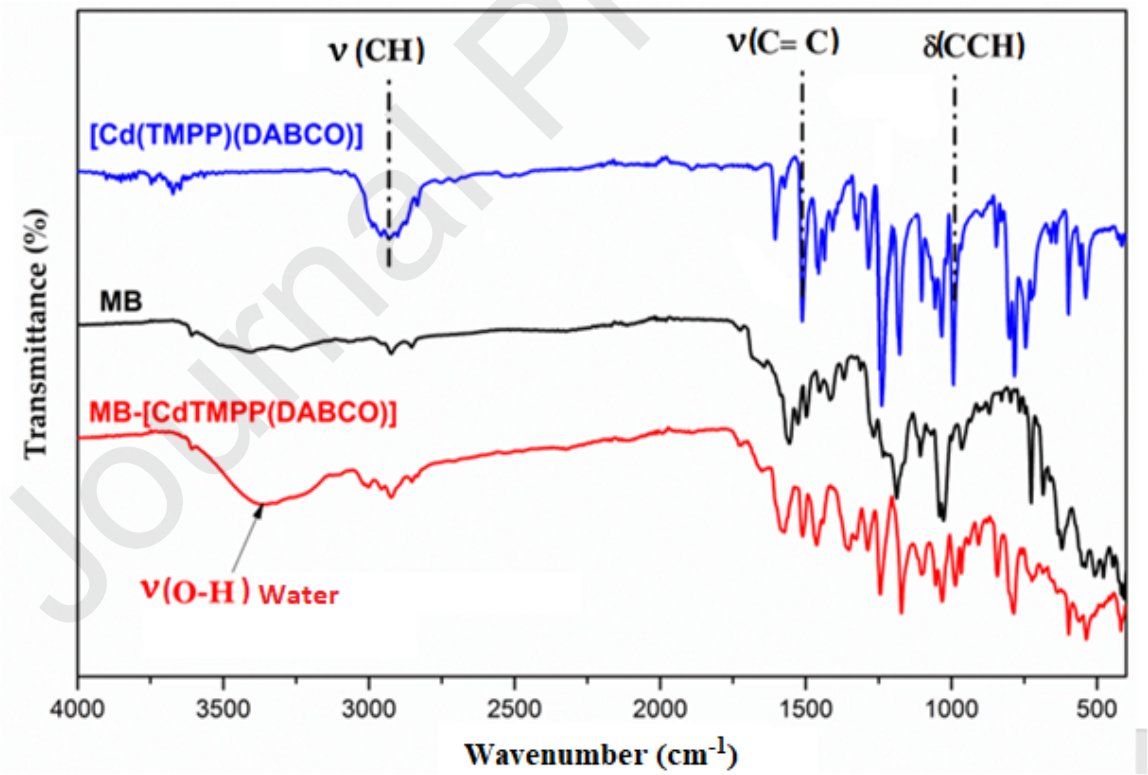

Figure 8. FT-IR spectra of [Cd(TMPP)(DABCO)], MB, and MB-[Cd(TMPP)(DABCO)].

Table 9. Important FT-IR data (cm−1) of [Cd(TMPP)(DABCO)], MB, and MB-[Cd(TMPP)(DABCO)].

Assignment (functional groups)	**MB**	**[Cd(TMPP)(DABCO)](I)**	**MB-[Cd(TMPP)(DABCO)]**
ν(H_2O)	**-**	-	3360
ν(C-H)	[2957-2856]	[2987-2837]	[2995-2847]
ν(C=C)	1565	1511 (1532) *	1572(1530) *
ν(C-N) Ar	1369(1364)*	1330 (1332) *	1362 (1363) *
δ(CCH)	963 (977)*	977 (988) *	964 (978) *

(*) From the DFT vibrational frequency calculations

4. Conclusion

In summary, we have presented here the synthesis, the crystal structure and the photophysical properties of the (DABCO)(*meso*-tetrakis(4-tert-methoxyphenyl)porphyrinato)cadmium(II) (Complex (**I**)). The supramolecular assembly of this complex is made by weak non-conventional hydrogen bonds type C—H···N and C—H···O. Absorption spectra reveal that the insertion of Cd(II) metal ion into the TMPP porphyrinate and the addition of the DABCO axial ligand are accompanied by a redshift of the Soret and Q bands. While the Q bands of fluorescence emission spectra are blue shifted with a decrease of the fluorescence intensity, quantum yield (φ_f) and lifetime (τ_f). This quenching of the fluorescence is explained by the "heavy-atom effect" of the cadmium heavy metal. Cationic MB dye adsorption removal from aqueous solution using our synthetic cadmium(II)-DABO porphyrin derivative yield an adsorption capacity of 69.24 $mg.g^{-1}$. DFT simulations on the interaction of MB and DABCO on complex (I) was lower than the interaction of DABCO alone (exothermic behavior), this is in agreement with experimental finding. FT-IR characterization was used to confirm the adsorption of the MB dye molecule in [Cd(TMPP)(DABCO)].

These promising results obtained using our Cd(II)-TMPP-DABCO system pave the way for us to test other cadmium porphyrin complexes but using other *meso*-arylporphyrins as well as other types of axial ligands in order to improve the adsorption treatments of organic dyes on wastewater..

Supporting information

CCDC 2012300 contain the supplementary crystallographic data of complex **(I).** These data can be obtained free of charge from the Cambridge Crystallographic Data Centre viawww.ccdc.cam.ac.uk/data_request/cif.

Acknowledgements

The authors gratefully acknowledge financial support from the Ministry of Higher Education and Scientific Research of Tunisia.The authors extend their appreciation to the deanship of Scientific Research at Majmaah

University, Saudi Arabia. A.J. is grateful to the High-Performance Computing Center (Aziz Supercomputer) at King Abdulaziz University (KAU) for the resources and the support.

References

[1] K. Yu, P. Puthiaraj, W. S. Ahn, One-pot catalytic transformation of olefins into cyclic carbonates over an imidazolium bromide-functionalized Mn(III)-porphyrin metal–organic framework, *Applied Catalysis B: Environmental,* **2020***,* 273,119059.

[2] Z. Yang, L. Fan, X. Fan, M. Hou, Z. Cao, Y. Ding, and W. Zhang, Porphyrin-GO Nanocomposites Based NIR Fluorescent Sensor Array for Heparin Sensing and Quality Control, *Anal. Chem*.,**2020**, 92, 9, 6727–6733.

[3] Satrialdi, R. Munechika, V. Biju, Y. Takano, Cd Hideyoshi Harashimaa and Yuma Yamada, Correction: The optimization of cancer photodynamic therapy by utilization of a pi-extended porphyrin-type photosensitizer in combination with MITO-Porter, *Chem. Commun.*, **2020**, 56, 6153-6153.

[4] K. Zeng, Z. Tong, L. Ma, W. H. Zhu, W. Wu, and Y. Xie, Molecular engineering strategies for fabricating efficient porphyrin-based dye-sensitized solar cells, *Energy Environ. Sci*., **2020**, 13, 1617-1657.

[5] Z. Valicsek, O. Horváth, G. Lendvay, I. Kikaš, I. Škorić, Formation, photophysics, and photochemistry of cadmium(II) complexes with 5,10,15,20-tetrakis(4sulfonatophenyl)porphyrin and its octabromo derivative: the effects of bromination and the axial hydroxo ligand, *J. Photochem. Photobiol.* A., **2011**,218, 143–155.

[6] Z. Valicsek, O. Horváth, Application of the electronic spectra of porphyrins for analytical purposes: The effects of metal ions and structural distortions, *Microchem. J*., **2013**,107, 47–62.

[7] E. Nyarko, M. Tabata, Interactions of Tetracationic Mercury (II), Cadmium (II) and Lead (II) Porphyrins with DNA and their Effects on DNA Cleavage. *J. Porphyrins Phthalocyanines,* **2001**, *5*, 873-880.

[8] M. Tabata, A. Kumar Sarkar, E. Nyarko, Enhanced Conformational Changes in DNA in the Presence of Mercury(II), Cadmium(II) and Lead(II) Porphyrins. *J. Inorg. Biochem.***2003**, 94, 50-58.

[9] E. Nyarko, T. Hara, D. J. Grab, M. Tabata, T. Fukuma, Toxic Effects of Mercury(II), Cadmium(II) and Lead(II) Porphyrins on *Trypanosoma Brucei Brucei* Growth. *Chem. Biol. Interact.***2002**, 139, 177-185.

[10] H. Ucun, Equilibrium, thermodynamic and kinetics of reactive black 5 biosorption on loquat (Eriobotrya japonica) seed, *Sci. Res. Essays*, **2011**, 19, 4113–4124.

[11] E. Makhado, S. Pandey, K. Desmond Modibane, M. Kang, M. Joseph Hato, Sequestration of methylene blue dye using sodium alginate poly(acrylic acid)@ZnO hydrogel nanocomposite: Kinetic, Isotherm, and Thermodynamic Investigations, *Int. J. Biol. Macromol*, **2020**, 162, 60-73.

[12] S. Pandey, J. Y. Do, J. Kim, M. Kang, Fast and highly efficient removal of dye from aqueous solution using natural locust bean gum based hydrogels as adsorbent, *Int. J. Biol. Macromol*, **2020**, 143, 60-75.

[13] A. S. Elfeky, S. Salem, A. S. Elzaref, M. E. Owda, H. A. Eladawy, A. M. Saeed, M. A. Awad, R. E. Abou-Zeid, A. Fouda Multifunctional cellulose nanocrystal /metal oxide hybrid, photo-degradation, antibacterial and larvicidal activities, *Carbohydr. Polym.* **2020**, 230, 115597.

[14] S. Pandey, K. K. Mandari, J. Kim, M. Kang, E. F. Kankeu, Photocatalysts in Advanced Oxidation Processes for Wastewater Treatment in book: Photocatalysts in Advanced Oxidation Processes for Wastewater Treatment, Chapter, **2020**, 6, 167-196.

[15] K. Mahapatra, D. S. Ramteke, L. J. Paliwal, Production of activated carbon from sludge of food processing industry under controlled pyrolysis and its application for methylene blue removal, *J. Anal. Appl. Pyrolysis*, **2012**;95, 79–86.

[16] X. Ma, M. Chao, Rapid voltammetric determination of maltol in some foods and beverages using a poly(methylene blue)/graphene-modified glassy carbon electrode, *J. Solid State Electrochem*., **2014,** 3, 621–628.

[17] S. Yan, H. Zhang, Z. Yang, M. Tang, M. Zhang, C. Du, H. L. Cui, D. Wei, Transformation and dehydration kinetics of methylene blue hydrates detected by terahertz time-domain spectroscopy, RSC Adv., **2017**, 7, 41667–41674.

[18] S. Cengiz, S., L. Cavas, Removal of methylene blue by invasive marine seaweed: Caulerparacemosa var. cylindracea, *Bioresource Technology*, **2008**, 99, 2357–2363.

[19] A. S. Alzaydien, , Adsorption of methylene blue from aqueous solution onto a low cost natural Jrdanian Tripoli, *American Journal of Environmental Sciences*, **2009**, 5,197–208.

[20] P.C.C. Faria, J.J. Mórfão, M.F.R. Pereira, Adsorption of anionic and ˜ cationic dyes on activated carbons with different surface chemistries, *Water Res*., **2004**, 38, 2043–2052.

[21] J. Zhang, A. Wang, Adsorption of Pb(II) from Aqueous Solution by Chitosan-g-poly(acrylic acid)/ Attapulgite/Sodium Humate Composite Hydrogels*, J. Chem. Eng. Data*, **2010**, 55, 2379.

[22] L. Zhu, L. Zhang, Y. Tang, X. Kou, Synthesis of Sodium Alginate Graft Poly (Acrylic Acid-Co-2-Acrylamido-2-Methyl-1-Propane Sulfonic Acid)/Attapulgite Hydrogel Composite and the Study of its Adsorption, *Polym. Plast. Technol. Eng*. **2014**, 53, 74.

[23] K.I. Aly, M. M. Sayed, M. G. Mohamed, , S. W. Kuo, O. Younis, A facile synthetic route and dual function of network luminescent porous polyester and copolyester containing porphyrin moiety for metal ions sensor and dyes adsorption, *MICROPOR MESOPOR MAT*, **2020**, 298, 110063.

[24] Y. Hou, J. Sun, D. Zhang, D. Qi,and J. Jiang, Porphyrin–Alkaline Earth MOFs with the Highest Adsorption Capacity for Methylene Blue, *Chem. Eur. J.* **2016**, 22, 6345 – 6352:

[25] R. Soury, M. Jabli, T. A. Saleh, W. Sattar A. Hassan, E. S.-Aman, F. Loiseau, Ch. Philouze and H. Nasri Tetrakis(ethyl-4(4-butyryl)oxyphenyl)porphyrinato zinc complexes with 4,40bpyridin: synthesis, characterization, and its catalytic degradation of Calmagite, , *RSC Adv*., **2018**, 8, 20143–20156.

[26] M. Guergueb, J. Brahmi, S. Nasri, F. Loiseau, K. Aouadi, V. Guerineau, S. Najmudin and H. Nasri Zinc(II) triazole meso-aryl substituted porphyrins for UV-visible chloride and bromide detection. Adsorption and catalytic degradation of malachite green dye, *RSC Adv*., **2020**, 10, 22712–22725,

[27] M. Guergueb, S. Nasir, J. Brahmi, F. Loiseau, F. Molton, T. Roisnel, V. Guerineau, I. Turowska-Tyrk, K. Aouadi and H. Nasri, Effect of the coordination of p-acceptor 4-cyanopyridine ligand on the structural and electronic properties of meso-tetra(para-methoxy) and meso-tetra(para-chlorophenyl) porphyrin cobalt(II) coordination compounds. Application in the catalytic degradation of methylene blue dye, *RSC Adv*., **2020,** 10, 6900–6918.

[28] A. D. Adler, F. R. Longo, J.D. Finarelli, J. Goldmacher, J. Assour, L. J. Korsakoff, A Simplified Synthesis for Meso-Tetraphenylporphine, *Org Chem*, **1967**,32, 476.

[29] P. F. Rodesiler, E. A. H. Griffith, N. G. Charles, L. Lebioda, E. L. Amma, Molecular Distortions and Solid-state 113Cd NMR: Crystal and Molecular Structure of the Piperidine Adduct of (5,10,15,20-Tetraphenylporphyrinato)cadmium(II), ^{113}Cd NMR Solution and Solid-state Spectra, and Potential Energy Calculations, *Inorg. Chem,***1985**, 24, 4595-4600.

[30] P. G. Seybold, M. Gouterman, Fluorescence Spectra and Quantum Yields, *J. Mol. Spectrosc*, **1969**,31,1-13.

[31] P. J. Becker, P. Coppens, Extinction within the limit of validity of the Darwin transfer equations. I. General formalism for primary and secondary extinction and their applications to spherical crystals, *Acta Crystallogr.***, *A30,*1974**,129-147.

[32] M. C. Burla, R. Caliandro, M. Camalli, B. Carrozzini, G. L. Cascarano, L. De Caro, C. Giacovazzo, G. Polidori, R. Spagna, SIR2004: an improved tool for crystal structure determination and refinement, J. Appl. Cryst, **2005**, 38, 381-388.

[33] G. M. Sheldrick, Crystal structure refinement with SHELXL, *Acta Cryst. A64,***2008** 112-122.

[34] P. G. Byrom, B. W. Lucas,*PARSET* and *PARSYM* - production of files for neutron powder structure refinement program *MORGUE* and solution/refinement program *PARAM*, *J. Appl. Cryst.*,**1995**, 28, 65-66

[35] C. F. Macrae, I. J. Bruno, J. A. Chisholm, P. R. Edgington, P. McCabe, E. Pidcock, L. Rodriguez-Monge, R. Taylor, J. Van Der Streek, P. A, Wood, Mercury CSD 2.0 - New Features for the Visualization and Investigation of Crystal Structures. *J. Appl. Cryst,***2008**, 41, 466-470.

[36] S. Lagergren, about the theory of so-called adsorption of soluble substances, Kungliga Suensk Vetenskapsakademiens Handling, **1898**, 241, 1–39.

[37] G. Blanchard, M. Maunaye, G. Martin, Removal of heavy metals from waters by means of natural zeolites, *Water Res*.,**1984**, 18, 1501–1507.

[38] M. Lintock, The Elovich equation in chemisorption kinetics. *Nature,* **1967**, 216, 1204-1205.

[39] I. Langmuir, The adsorption of gases on plane surfaces of glass, mica, and platinum, *J. Am. Chem. Soc.*,**1918**, 40, 1361–1403.

[40] H. M. F. Freundlich, Adsorption in solution, *Phys. Chem. Soc*., **1906**, 40, 1361–1368.

[41] O**.** Redlich, D. L. Peterson, A useful adsorption isotherm. *J. Phys. Chem.*,**1959**, 63 (6),1024.

[42] H. N. Tran, S. J.You, A. H. Bandegharaei, H.P. Chao Mistakesand inconsistencies regarding adsorption of contaminants fromaqueous solutions: a critical review. *Water Res,* **2017**, 120, 88–116.

[43] M. J. Frisch, G.W.Trucks, H. B. Schlegel, G. E. Scuseria, M. A. Robb, J. R. Cheeseman, G. Scalmani, V. Barone, B. Mennucci, G. A. Petersson, Gaussian 09; revision A.02; Gaussian, Inc.: Wallingford, CT, USA, **2009**.

[44] R. Dennington R, T. Keith, J. Millam , *GaussView. Version 5, vol Shawnee Mission. Semichem. Inc*. **2009**.

[45] P.J. Stephens, F.J. Devlin, C.F. Chabalowski, M.J. Frisch, *J. Phys. Chem.,* **1994**, 98, 11623-11627.

[46] D. Moran, A. C. Simmonett, F. E. Leach, W. D. Allen, P. v. R. Schleyer, H. F. Schaefer "Popular theoretical methods predict benzene and arenes to be nonplanar". *J. Am. Chem. Soc.,* **2006,** 128 (29), 9342–9343.

[47] M. Dolg, H. Stoll, and H. Preuss, "Energy-adjusted ab initio pseudopotentials for the rare earth elements," *J. Chem. Phys*., **1989**, 90 1730-34.

[48] S. Miertus, J. Tomasi, *Chem. Phys*., **1982**, 65, 239.

[49] K. Wolinski, J. F. Hinton, P. Pulay, Efficient Implementation of the Gauge-Independent Atomic Orbital Method for NMR Chemical Shift Calculations. *J Am Chem Soc.* **1990**, 112(23),8251–60.

[50] A. W. Addison, T. N. Rao, J. Reedijk, J. van Rijn, G. C. Verschoor, Synthesis, structure, and spectroscopic properties of copper(II) compounds containing nitrogen–sulphur donor ligands; the crystal and molecular structure of aqua[1,7-bis(*N*-methylbenzimidazol-2′-yl)-2,6-dithiaheptane]copper(II) perchlorate,*J. Chem. Soc., Dalton Trans.*, **1984**, 1349-1356.

[51] C. Mchiri, H. Nasri, C. Frochot, S. Acherar, Distorted five-coordinate square pyramidal geometry of a cadmium(II) complex containing a 2-methylimidazole ligand: Crystal structure and axial ligand effect on spectroscopic properties, *Polyhedron, **2019**,* 173,107-114.

[52] W.-S. Wun, J.-H. Chen, S.-S. Wang, J.-Y. Tung, F.-L. Liao, S.-L. Wang, L.-P. Hwang, S. Elango, chlorophenyl)porphyrinato](pyridine)cadmium(II) pyridine solvate and [meso-tetra-(p-chlorophenyl)porphyrinato](dimethylformamide)cadmium(II) toluene solvate**,** *Inorg. Chem. Commun*., **2004**,7, 1233–1237.

[53] P. F. Rodesiler, E. A. H. Griffith, N. G. Charles,t L. Lebioda, and E. L. Amma, Molecular Distortions and Solid-state ‘13Cd NMR: Crystal and Molecular Structure of the Piperidine Adduct of (5,10,15,20-Tetraphenylporphyrinato)cadmium(II), ‘^{13}Cd NMR Solution and Solid-state Spectra, and Potential Energy Calculations, Inorg. Chem. **1985**, 24, 4595-4600.

[54] M. P. Byrn, C. J. Curtis, Yu. Hsiou, S. I. Khan, P. A. Sawin, S. K. Tendick, A. Terzis, C. E. Strouse, Porphyrin sponges: conservative of host structure in over 200 porphyrin-based lattice clathratesJ.Am.Chem.Soc, **1993**, 115, 9480.

[55] P. S. Zhao, F. F. Jian, L. Zhang, Synthesis, Characterization and Crystal Structure of (α-Aminopyridine-N)-(5,10,15,20-tetraphenylporphyrinato) Cadmium(II) Acetone Solvate, *Bull. Korean Chem. Soc*., **2006**, 27, 1053–1055.

[56] H. Toumi, N. Amiri, M. S. Belkhiria, J.-C. Daran, H. Nasri, Di-μ-azido-bis(μ-1,4,7,10,13,16-hexaoxacyclooctadecane)bis(5,10,15,20-tetraphenylporphyrinato)dicadmiumdisodium, *Acta Crystallogr. Sect. E Struct. Rep. Online*, **2012**,68, 1557–1158.

[57] D. R. Reddy B. G. Maiya, Bis(aryloxo) derivatives of tin(IV) porphyrins: synthesis, spectroscopy and redox activity, *J. Porphyrins Phthalocyanines*, **2002**, 6 (1), 3-11.

[58] A. A. Kumar, L. Giribabu, D. R. Reddy, B. G. Maiya, New molecular arrays based on a Tin (IV) porphyrin scaffold, *Inorg. Chem*., **2001**, 40, 6757-6766.

[59] S. Gentemann, C. J. Medforth, T. Ema, N.Y. Nelson, K.M. Smith, J. Fajer, D. Holten, Unusual picosecond 1 (π, π *) deactivation of ruffled nonplanar porphyrins, *Chem. Phys. Lett*., **1995**, 245, 441-447.

[60] Ti. Liu, L. Jing, L. Cui, Q. Y. Liu, X. Zhang, Facile One-pot Synthesis of A Porphyrin-based Hydrophilic Porous Organic Polymer and Application as Recyclable Absorbent for Selective Separation of Methylene Blue, *Chemosphere*, **2018**, 212, 1038-1046.

[61] Y. Hou, J. Sun, D. Zhang, D. Qi, and J. Jiang**,** Porphyrin–Alkaline Earth MOFs with the Highest Adsorption Capacity for Methylene Blue, *Chem. Eur. J*. **2016**, 22, 6345 – 6352.

[62] Y. Miyaha, A. Lahrichib, M. Idrissi, Removal of cationic dye –Methylene bleu– from aqueous solution by adsorption onto corn cob powder calcined.*J. Mater. Environ. Sci., **2016**, 7 1,96-104.*

[63] F. Z. Batana, M. B. Taouti , A. Guibadj, Cinétique de l'adsorption du bleu de méthylène sur bentonite brute et traitée, *Algerian Journal of Environmental Science and Technology December edition.* **2019**, 5(4).

[64] S**.** Farhadi, M. Dusek, F. Siadatnasab, V. Eigner, A. M. andani, First organic-inorganic hybrid nanomaterial constructed from a Keggin-type polyoxometallate and a copper-dithiocarbamate complex: sonochemical synthesis, crystal structure and its adsorption performance for organic dye pollutants, *Polyhedron*, **2017**, 126, 227-238.

Conflict of interest

All Authors declares that thereis no conflict of interest.

Highlights

- ✓ Synthesis of the DABCO-tetrakis[4(methoxy)phenylporphyrin] cadmium complex.
- ✓ Molecular structure was determined by single crystal X-Ray diffraction technique.
- ✓ Density Functional Theory (DFT) have been used for calculations on the structure, ^{1}H NMR spectroscopy and IR spectra analysis.
- ✓ UV–visible and Fluorescence investigations were made.

✓ Adsorption removal of methylene blue using our Cd-DABCO-porphyrin compound.